ROS Fusion Tyrosine Kinase Activates a SH2 Domain–Containing Phosphatase-2/Phosphatidylinositol 3-Kinase/Mammalian Target of Rapamycin Signaling Axis to Form Glioblastoma in Mice

Al Charest,[1] Erik W. Wilker,[1] Margaret E. McLaughlin,[2] Keara Lane,[1] Ram Gowda,[1] Shanie Coven,[1] Kevin McMahon,[1] Steven Kovach,[1] Yun Feng,[1] Michael B. Yaffe,[1] Tyler Jacks,[1] and David Housman[1]

[1]Department of Biology and Center for Cancer Research, Massachusetts Institute of Technology, Cambridge, Massachusetts and [2]Brigham and Women's Hospital, Department of Pathology, Boston, Massachusetts

Abstract

Glioblastoma multiforme is the most common and lethal form of primary brain cancer. Diagnosis of this advanced glioma has a poor prognosis due to the ineffectiveness of current therapies. Aberrant expression of receptor tyrosine kinases (RTK) in glioblastoma multiformes is suggestive of their role in initiation and maintenance of these tumors of the central nervous system. In fact, ectopic expression of the orphan RTK ROS is a frequent event in human brain cancers, yet the pathologic significance of this expression remains undetermined. Here, we show that a glioblastoma-associated, ligand-independent rearrangement product of ROS (FIG-ROS) cooperates with loss of the tumor suppressor gene locus *Ink4a;Arf* to produce glioblastomas in the mouse. We show that this FIG-ROS-mediated tumor formation *in vivo* parallels the activation of the tyrosine phosphatase SH2 domain–containing phosphatase-2 (SHP-2) and a phosphatidylinositol 3-kinase/Akt/mammalian target of rapamycin signaling axis in tumors and tumor-derived cell lines. We have established a fully penetrant preclinical model for adult onset of glioblastoma multiforme in keeping with major genetic events observed in the human disease. These findings provide novel and important insights into the role of ROS and SHP-2 function in solid tumor biology and set the stage for preclinical testing of targeted therapeutic approaches. (Cancer Res 2006; 66(15): 7473-81)

Introduction

Glioblastoma multiforme is the most common subtype of malignant primary brain cancer. Each year, glioblastoma multiformes are responsible for a significant number of deaths, as they claim the lives of >80% of patients within the first year after diagnosis (1). The deadly nature of glioblastoma multiformes resides in their high rate of cell proliferation and extremely invasive behavior. Despite efforts to develop novel therapies, the survival rates have changed little in the past few decades, reflecting the innate resistance of glioblastoma multiformes to surgical approaches, chemotherapeutics, and radiation therapy. Individualized molecularly tailored therapies in conjunction with standard treatments represent a promising approach to long-term disease management.

The orphan RTK ROS exhibits a restricted pattern of expression in mammals, where it has been suggested to play a role in mesenchymal-to-epithelial transition during the development of kidney, lung, and small intestine (2–4). The c-ROS receptor has been reported to be ectopically expressed in 30% of human glioma cell lines and tumors, suggesting ROS may contribute to glioma initiation and/or maintenance (5–10). However, the consequences of ectopic ROS expression on tumorigenesis have never been addressed experimentally. We recently characterized a small interstitial microdeletion on 6q21 in two human glioblastoma cell lines that result in the fusion of a Golgi apparatus–associated protein, called FIG, to the kinase domain of ROS (11, 12). We also showed that the result of this event is similar to the intragenic deletion of exons 2 to 7 of the epidermal growth factor receptor (known as vIII) found in a substantial percentage of glioblastoma multiformes, which is the creation of a constitutively activated ligandless version of its cognate full-length receptor. The hybrid FIG-ROS kinase is a potent oncogene *in vitro*, readily transforming Rat1 fibroblasts through its ability to accumulate at the Golgi apparatus, which results in constitutive tyrosine kinase activity (11).

Germ-line mutations of the *Ptpn11* gene that codes for the SH2 domain–containing tyrosine phosphatase SHP-2 are associated with Noonan syndrome, an autosomal dominant disorder associated with an increased incidence of leukemia (13). Somatic *Ptpn11* mutations have been observed in a high percentage of hematologic malignancies (14–17). Recently, mutations in *Ptpn11* have been found in solid tumors of the lung, colon, peripheral nervous system, and skin (18). All of the observed mutations predict an activated form of SHP-2, suggesting that constitutive activation of SHP-2 is an oncogenic event. Consistent with this observation, transduction of mouse bone marrow cells harboring a constitutively active SHP-2 mutation causes a fatal JMML-like disorder *in vivo* (19).

To ascertain the role of ROS RTK in brain tumor formation and signal transduction pathways in this context, we investigated the ability of a surrogate activated version of ROS (FIG-ROS) to generate primary brain tumors *in vivo*. We created a *FIG-ROS* conditional mouse strain (referred to as *LSL-FIG-ROS*), in which expression of FIG-ROS kinase is controlled by a Cre recombinase–mediated removal of a transcriptional termination stop cassette. Stereotactical injection of an adenovirus transducing Cre recombinase excises the stop element, which results in FIG-ROS expression. Here, we show that FIG-ROS expression leads to the formation of glioblastomas and that formation of these tumors is greatly

Note: Supplementary data for this article are available at Cancer Research Online (http://cancerres.aacrjournals.org/).

Requests for reprints: Al Charest or David Housman, Center for Cancer Research, Massachusetts Institute of Technology, E17-536, 77 Massachusetts Avenue, Cambridge, MA 02139. Phone: 617-253-3020; Fax: 617-253-5202; E-mail: charest@mit.edu or dhousman@mit.edu.

doi:10.1158/0008-5472.CAN-06-1193

accelerated in the absence of tumor suppressor genes *p16Ink4a; p19Arf*, the latter being an event observed in upward to 40% of human glioblastoma multiformes. Finally, we show that FIG-ROS-mediated tumor formation parallels activation of a SHP-2/phosphatidylinositol 3-kinase (PI3K)/Akt/mammalian target of rapamycin (mTOR) signaling pathway *in vivo*.

Materials and Methods

Conditional transgene construction and generation of mice. To construct the pCAGGS-LSL-FIG-ROS transgene, the CAGGS promoter (20) was cloned adjacent to a FIG-ROS SV40 poly(A) tail cDNA. A modified transcriptional/translational stop cassette (pBS302 plasmid; Invitrogen Life Technologies, Inc., Carlsbad, CA) was inserted between the CAGGS promoter and the FIG-ROS cDNA. The final plasmid was linearized and electroporated in embryonic stem cells; selected clones were screened for single integration events by Southern blot hybridization. Three individual clones were selected for production of chimeric animals and ensuing germ line–transmitted transgenic mice. One line (puro5) was crossed to InkΔ2/3 null animals (21) to generate compound transgenic mice.

Stereotactic injections. All of the mice used in this study were maintained and handled under protocols approved by the Committee on Animal Care at the Massachusetts Institute of Technology. Adult animals were anesthetized, mounted in a Stoelting stereotaxic frame (Harvard Apparatus Inc.), and a 1-mm burr hole was drilled at the stereotactically defined location of the striatum (2.1 mm rostral to the bregma, 1.5 mm lateral to the midline, and at 2-mm depth to the pia surface.). A 1-μL Hamilton syringe was used to inject adeno-CMV-Cre viruses (Gene Transfer Vector Core, University of Iowa) at a rate of 0.05 μL/min.

Histologic analysis of tumors, immunohistochemistry, and antibodies. Immunohistochemical staining was done using ABC system (Vector); 3,3′-diaminobenzidine staining and hematoxylin counterstaining were done according to the protocols of the manufacturer. The primary antibodies used were anti–glial fibrillary acidic protein (Dako, Carpinteria, CA), synaptophysin (Dako), Ki67 (Novocastra, Newcastle upon Tyne, United Kingdom), SMA (Dako), SHP-2 (Santa Cruz Biotechnology, Santa Cruz, CA), phosphotyrosine (BD Transduction Laboratories, Franklin Lakes, NJ), and anti-FIG (22).

Two-dimensional gel electrophoresis analysis of phosphoproteome. Whole-cell extracts were immunoprecipitated overnight with 4G10-conjugated agarose (Upstate Biotechnology, Charlottesville, VA), washed, eluted at 4°C in 8 mol/L urea, 2 mol/L thiourea, 4% CHAPS, 15 mmol/L Tris (pH 8.5), and labeled with 250 pmol/L of Cy2 (mutant FIG-ROS Y805,865F) or Cy3 (FIG-ROS) for 30 minutes on ice. For two-dimensional electrophoresis, labeled samples were combined and cup-loaded onto a 24-cm immobilized pH gradient (IPG) strip (pH 3-10), and subjected to isoelectric focusing using an IPGphor isoelectric focusing system device (Amersham Biosciences, Piscataway, NJ). Strips were washed and electrophoresed onto 6% to 20% SDS-PAGE gels. Gels were imaged on a 9400 Typhoon laser Variable Mode Imager (Amersham Biosciences) to visualize Cy2 (red) and Cy3 (green; Supplementary Fig. S4) labeled proteins. They were transferred onto polyvinylidene difluoride membranes and used for Western blot analyses using the indicated antibodies and detected by enhanced chemiluminescence (Renaissance, NEN-Dupont, Boston, MA).

***In vitro* binding studies.** The glutathione *S*-transferase (GST)-SH2(N) fusion protein of SHP-2 was expressed in bacteria and affinity purified on glutathione-sepharose beads (Pharmacia Biotech, Inc., Piscataway, NJ) according to published protocol (23). Cell lysates from COS-1 [+/− expressing myc-tagged FIG-ROS wild-type (WT), kinase dead (K511 M), and phosphorylation site mutants] or clonally derived Rat1 FIG-ROS variant cells were incubated with the GST fusion protein bound to glutathione-sepharose beads, washed, separated by SDS-PAGE, and immunoblotted or stained with Coomassie brillant blue (Bio-Rad, Hercules, CA).

Generation of tumor cell lines and growth inhibition assays. Tumors were excised, minced in 0.25% trypsin (wt/vol) 1 mmol/L EDTA, then allowed to dissaggregate for 15 minutes at 37°C, centrifuged, washed, and plated on 0.2% gelatin–coated tissue culture plates. Cells were starved overnight in 0.1% fetal bovine serum (FBS) and treated with wortmanin, LY294002, or rapamycin (Cell Signaling Technology Inc., Danvers, MA) at the indicated concentrations for 3 hours before addition of FBS at 20% final concentration. The 2,3-bis[2-methoxy-4-nitro-5-sulfophenyl]-2*H*-tetrazolium-5-carboxanilide inner salt growth assays were done according to the protocol of the manufacturer (Roche Applied Science, Penzberg, Germany). Cells were harvested and lysates separated by SDS-PAGE and Western blotted against the indicated proteins.

Results

Somatic induction of FIG-ROS expression in conditional transgenic mice. To investigate the physiologic results of aberrant ROS expression, we used a ligand-independent, constitutive active variant allele of ROS (i.e., FIG-ROS). We controlled FIG-ROS expression through an *in vivo* introduction of Cre recombinase by creating a conditional FIG-ROS transgenic animal in which a loxP site flanked transcriptional/translational stop cassette was inserted between a ubiquitous promoter and the FIG-ROS cDNA (Fig. 1*A*). Linearized transgene DNA was electroporated into embryonic stem cells, which were drug selected and screened for single transgene integration events by Southern blot analysis of embryonic stem cell genomic DNA (Supplementary Fig. S1*A*). Selected embryonic stem cell clones were injected into blastocysts and ensuing germ line–transmitted transgenic founders tested for Cre-mediated FIG-ROS expression (Supplementary Fig. S1*B*).

To obtain a strict spatio-temporal control of FIG-ROS expression, we did stereotactic intracranial injections of adenovirus transducing Cre recombinase (AdCre). Recombinant adenoviruses have been shown to efficiently deliver genes of interest in a wide range of tissues. Adenoviruses remain episomal following infection of host cells, resulting in a transient expression of Cre recombinase with no potential for insertional mutagenesis. We injected AdCre in the basal ganglia (striatum) of WT and pCAGGS-LSL-FIG-ROS mice and monitored tumor formation and survival. Forty percent of the injected pCAGGS-LSL-FIG-ROS animals developed tumors between 30 and 55 weeks postinjection and had to be euthanized due to neurologic deterioration (mostly seizures; Fig. 1*B* and Supplementary Fig. S1*C*). None of the WT mice developed any observable phenotype over the same period of time. These results show that injection of AdCre in the striatum of our FIG-ROS conditional transgenic line resulted in the formation of lethal tumors.

Cooperation of FIG-ROS expression and *p16Ink4a* and *p19Arf* loss produces malignant astrocytomas *in vivo*. Molecular characterization of human astrocytomas reveals an accumulation of genetic aberrations in which tyrosine kinase oncogenes are activated concomitant with loss of tumor suppressor gene function, such as those encoded by the Ink4a/Arf locus, which is mutated in 30% to 40% of glioblastomas (24). The relatively long latency and low penetrance of tumor formation in the AdCre injected pCAGGS-LSL-FIG-ROS transgenic line (Fig. 1*B*) strongly suggested that additional genetic lesions are required for efficient tumor development. We crossed the conditional FIG-ROS transgenic line to a strain of mice that carried dually disrupted *p16Ink4a* and *p19Arf* genes (referred herein after as InkΔ2/3). Homozygous null mice for the Ink4a/Arf locus develop lymphomas and subcutis sarcomas at a median age of 30 weeks and have never been reported to develop glioma in their life span (21). Cohorts of double pCAGGS-LSL-FIG-ROS;InkΔ2/3 transgenic animals were subjected to stereotactic AdCre injections and were monitored for tumor formation and survival (Fig. 1*B*). When combined with InkΔ2/3 deficiency, expression of FIG-ROS resulted in highly aggressive

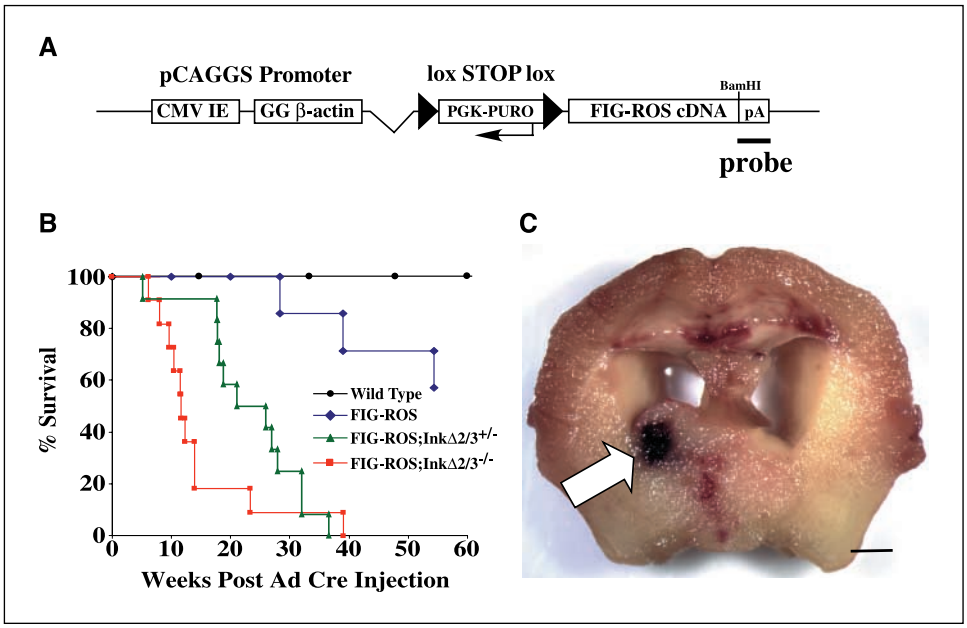

Figure 1. Localized somatic expression of FIG-ROS in adult mouse brains results in tumor formation. *A,* schematic representation of the conditional FIG-ROS transgene. *B,* tumor-free survival (Kaplan-Meier) analysis of AdCre-injected animal cohorts. Wild-type, $n = 6$; FIG-ROS, $n = 7$; FIG-ROS;InkΔ2/3$^{+/-}$, $n = 12$; and FIG-ROS;InkΔ2/3$^{-/-}$, $n = 11$. *C,* representative macroscopic features of a FIG-ROS;InkΔ2/3$^{+/-}$ tumor (*arrow*) 19 weeks post intracranial injection of AdCre. Bar, 1 mm.

tumor formation, significantly reducing the latency and increasing the penetrance of tumor formation, leading to death in 80% of the animals within 15 weeks after injection [$P < 0.0005$, comparing FIG-ROS to either pCAGGS-LSL-FIG-ROS;InkΔ2/3 genotype curve (log-rank test)]. FIG-ROS-expressing animals heterozygous for InkΔ2/3 locus also exhibited aggressive tumor formation albeit with a longer latency (Fig. 1*B*). This increase in latency is likely the result of time required for loss of the remaining wild-type *p16Ink4a;p19Arf* allele in the InkΔ2/3$^{+/-}$ animals. To address this issue, we isolated genomic DNA from FIG-ROS;InkΔ2/3$^{+/-}$ tumors and adjacent normal tissues and genotyped the *p16Ink4a;p19Arf* locus. All of the tumors analyzed displayed loss of heterozygosity at the *p16Ink4a;p19Arf* locus when compared with their normal matched control sample (Supplementary Fig. S2*A*).

Tumors resulting from AdCre-induced expression of FIG-ROS in the striatum of mice with *Ink4a;Arf* deletion appeared as masses with variable amounts of hemorrhage and compression of adjacent brain structures (Fig. 1*C, arrow*). At 4 weeks post AdCre injection, tumors were typically small (Fig. 2*A, Early, arrowheads*), often consisting of clusters of neoplastic cells (Fig. 2*B*). Over a period of an additional 4 weeks, the tumor masses increased rapidly in size (Fig. 2, *middle*). Interestingly, we did not observe changes in the cellular morphology in larger tumors when compared with early, smaller lesions (Fig. 2, *right*). In addition, we noticed a statistically significant difference in the progression of the disease within the cohort of FIG-ROS;InkΔ2/3 null animals. Older mice (>100 days old) that underwent AdCre injections succumbed to the developing tumors significantly more rapidly

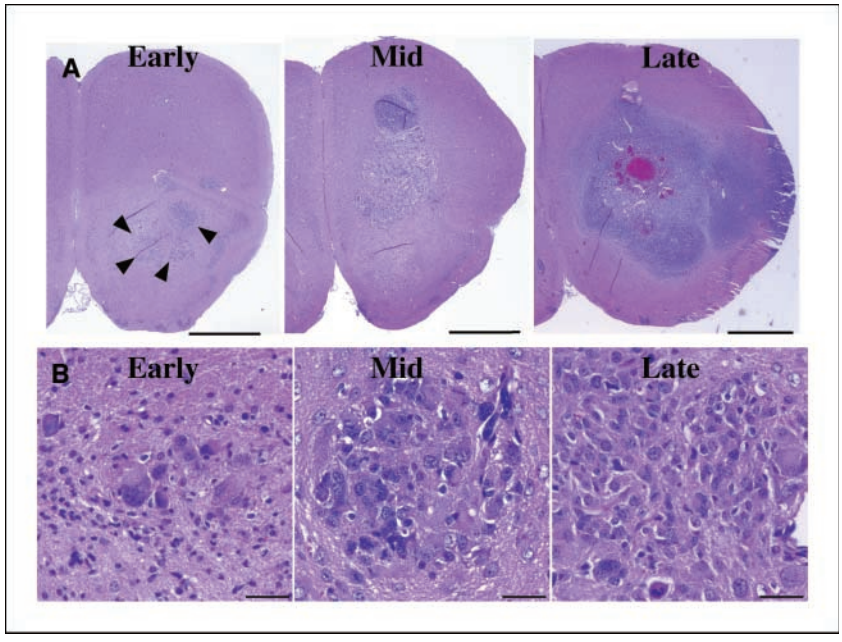

Figure 2. FIG-ROS tumors show growth characteristics similar to human malignant astrocytomas. *A,* representative time-course analysis of tumor progression in FIG-ROS;InkΔ2/3$^{-/-}$ mice. Brains were isolated at 4.2 (*Early*), 6.1 (*Mid*), and 8.7 (*Late*) weeks post AdCre injection and processed for analysis. Histologic sections of brains were examined for the presence of early-stage (*arrowheads*), mid-stage, and late-stage lesions. *B,* high-power magnification of lesions shown in (*A*). Bar, 1 mm (*A*) and 30 μm (*B*).

(mean of 68 days) than younger animals (<100 days old; mean, 102 days; Supplementary Fig. S2*B*).

The histopathologic features of FIG-ROS tumors are similar to human astrocytomas. FIG-ROS;InkΔ2/3 tumors are highly cellular and are composed of cells containing pleomorphic nuclei (Fig. 3*A, white arrows*). The tumors also contained variable numbers of larger, multinucleated cells [Fig. 3*A* (*arrowhead*) and Supplementary Fig. S3*D*]. Tumor cells typically have a gemistocytic appearance with eccentrically placed nucleus and abundant cytoplasm. The tumor cells are set in a fibrillary background (Fig. 3*A* and Supplementary Fig. S3*D*). Immunohistochemical staining for the astrocytic markers glial fibrillary acidic protein and S100β (Fig. 3*B* and Supplementary Fig. S3*E*, respectively) revealed that a subset of the neoplastic cells were expressing these markers of astrocytic differentiation but markers of neuronal lineage, such as synaptophysin, were absent (data not shown). The tumors contain a high number of proliferating cells as detected by the presence of mitoses (Fig. 3*A, black arrow*) and immunostaining with a MIB-1 (Ki67) antibody (Supplementary Fig. S3*F*). In addition, these tumors are highly vascularized (Supplementary Fig. S3*G*). The astrocytomas from this model are composed of a central mass with diffusely infiltrative margins. In the majority of tumors, a population of astrocytoma cells infiltrated the brain by migrating along subarachnoid and perivascular Virchow-Robin spaces (Fig. 3*C*), features often associated with malignant astrocytomas. Thirty percent of the FIG-ROS;InkΔ2/3 null tumors exhibited regions of necrosis (Fig. 3*D*), a feature characteristic of glioblastoma multiforme (or WHO grade 4 lesion). We also observed a FIG-ROS;InkΔ2/3 null tumor which exhibited features reminiscent of gliosarcoma (Supplementary Fig. S3), a glioblastoma multiforme variant characterized by a biphasic morphology with areas displaying either glial or mesenchymal differentiation. In total, 70% of the FIG-ROS;InkΔ2/3 tumors contain features similar to anaplastic astrocytomas (WHO grade 3) and 30% as glioblastoma multiformes (WHO grade 4; Supplementary Fig. S3*H*). Taken together, these results show that expression of FIG-ROS in central nervous system (CNS) glia cooperates with loss of the tumor suppressor locus *Ink4a;Arf* gene products to form brain tumors that behave like and are histologically similar to anaplastic astrocytomas and glioblastoma multiforme.

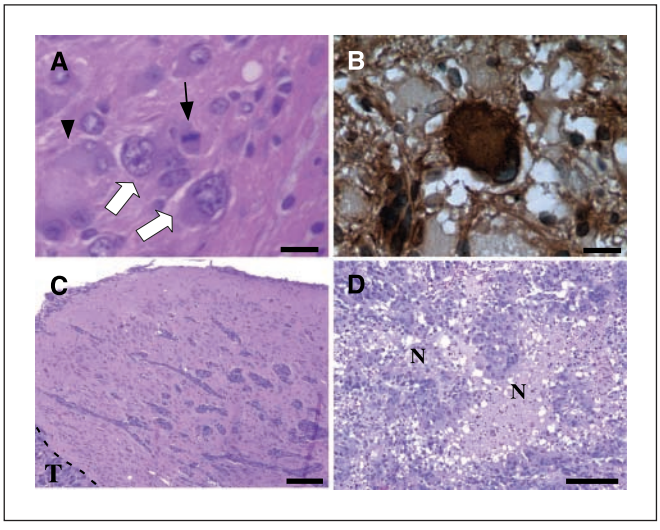

Figure 3. High-grade malignant astrocytoma in FIG-ROS;InkΔ2/3 null mice. Tumors show hallmarks of high-grade astrocytomas. *A,* H&E-stained brain tumor sections showing nuclear atypia (*white arrows*) and the presence of mitotic cells (*black arrow*) and large multinucleated cells (*arrowhead*). *B,* immunohistochemical characterization of FIG-ROS Ink4a/Arf null tumors showing positivity for glial fibrillary acidic protein, a marker of differentiated astrocytes. *C,* classic leptomeningial and perivascular invasion of tumor cells; *D,* pseudo palisading necrosis (*N*). Bar, 30 μm (*A* and *B*) and 125 μm (*C* and *D*).

Signaling pathways initiated by FIG-ROS in cancer cells. Tyrosine kinases relay signals through the phosphorylation of substrate molecules (reviewed in ref. 25). To better understand the mechanisms by which FIG-ROS exerts its oncogenic potential, we seek to identify FIG-ROS substrate(s) and interacting protein(s). We had previously shown that the ability of FIG-ROS to transform Rat1 cells *in vitro* can be eliminated by mutating two major autophosphorylation tyrosine residues within the COOH-terminal tail of FIG-ROS to phenylalanine (Y805,865F; ref. 11), which indicated that the signaling events emanating from these autophosphorylation sites are key to the capacity of FIG-ROS to transform cells. To search for tyrosine-phosphorylated proteins that specifically interacted with FIG-ROS through these two autophosphorylation sites, we did a phosphotyrosine proteome analysis from Rat1 cell extracts expressing WT or mutant (Y805,865F) FIG-ROS by Cy-dye label two-dimension PAGE analysis (Fig. 4). A relatively low number of minor differences between the two samples were observed except for the presence of a major species (Fig. 4*B, arrow*) corresponding to a protein of ~62-kDa molecular weight with an isoelectric point (p*I*) of 5.8, which was found to be preferentially phosphorylated in anti-phosphotyrosine immunoprecipitates from lysates of WT FIG-ROS when compared with the double phosphotyrosine FIG-ROS mutant (Y805,865F) in a reproducible manner.

To complement these results, we sought to identify effector proteins with phosphotyrosine binding SH2 and PTB domains capable of physically interacting with FIG-ROS through its Y805 and Y865 autophosphorylation sites by comparing their surrounding amino acid sequences to various recognition patterns of SH2 and PTB domains. We found that the SH2 domains of the tyrosine phosphatases SHP-2 and SHP-1 are expected to recognize and interact with pY805 and pY865 FIG-ROS. We tested the (NH2-) SH2 domain of SHP-2 for binding to FIG-ROS *in vitro* by GST-SH2 domain pulldown assays. We found that the (NH2-) SH2 domain of SHP-2 binds to FIG-ROS in a phosphotyrosine-dependent manner (Supplementary Fig. S5*A-C*). These results were validated by probing immunoprecipitates of SHP-2 from mammalian cells for the presence of FIG-ROS under conditions nondisruptive to protein interactions. We readily detected a phosphotyrosine-dependent association between endogenous SHP-2 and FIG-ROS (Fig. 4*C*). Interestingly, both FIG-ROS autophosphorylation sites (Y805 and Y865) represent recognition binding sites for the (NH2-) SH2 domain of SHP-2. The interaction between the SH2(N) domain of SHP-2 and FIG-ROS Y805 and/or Y865 residue was ascertained by GST pulldown assays. Both pY805 and pY865 are individually capable of mediating an *in vitro* interaction with the SHP-2 GST-SH2(N) proteins (Supplementary Fig. S5*D*). However, mutating both tyrosine residues simultaneously (Y805,865F) prevented the GST-SH2(N) fusion protein from binding, indicating that either FIG-ROS major autophosphorylation site is a target of the SH2(N) domain of SHP-2. Taken together, these results show that SHP-2 can interact with FIG-ROS in a tyrosine phosphorylation–dependent manner and that phosphorylation on either Y805 or Y865 site is sufficient to mediate this interaction.

The expected p*I* of SHP-2 is 5.8 and its calculated molecular weight is 68 kDa (migrating at ~62 kDa on SDS-PAGE). In line with

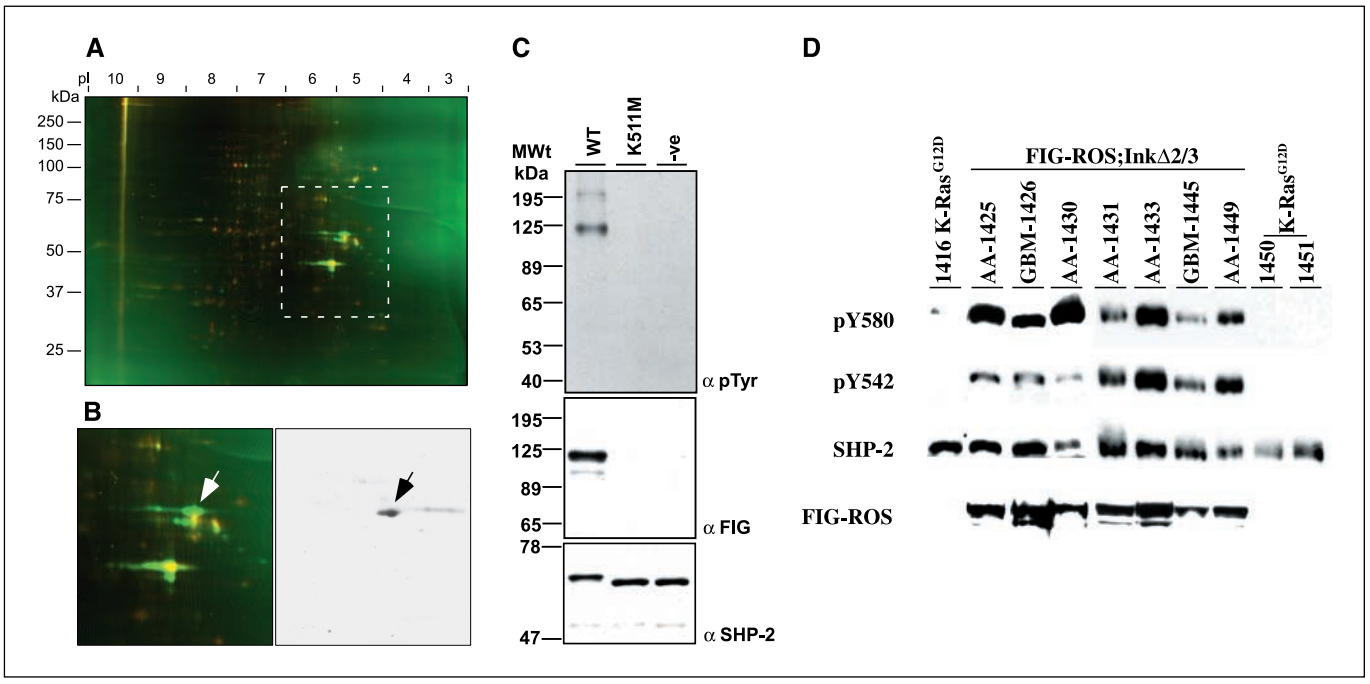

Figure 4. SHP-2 is a major phosphotyrosine protein in FIG-ROS transformed cells. *A* and *B,* two-dimensional PAGE phosphotyrosine proteome analysis of FIG-ROS-expressing cells. Lysates from FIG-ROS and FIG-ROS autophosphorylation mutant (Y805,865F) cells were immunoprecipitated with an anti-phosphotyrosine antibody and labeled individually with Cy2 (FIG-ROS; *green*) and Cy3 (FIG-ROS Y805,865F; *red*) dyes, mixed, and separated as described in Materials and Methods. *A,* representative of a merged image. *B, left,* close-up of (*A*) revealing a protein (*white arrow*) present in the FIG-ROS and not in the FIG-ROS Y805,865F extracts; *right,* Western blot analysis of the same area showing anti-SHP-2 immunoreactivity (*black arrow*). *C,* equi-amounts of lysates from COS-1 cells expressing WT FIG-ROS or a kinase inactive variant (K511M) were immunoprecipitated with an anti SHP-2 antibody and Western blotted using an anti-phosphotyrosine antibody (*top*) and an anti-FIG antibody (*middle*) that recognize FIG-ROS. Virgin COS-1 cells (*-ve*) were used as a negative control. A membrane containing total cell lysates from each samples was probed using an anti-SHP-2 antibody to control for the amount of SHP-2 proteins in the lysates (*bottom*). *D,* SHP-2 is phosphorylated on tyrosine residues Y580 and Y542 in tumor-derived astrocytoma cell lines expressing FIG-ROS. Lysates labeled as 1416, 1450, and 1451 were extracted from sarcoma cell lines expressing activated K-Ras^{G12D} and lysates labeled as AA-1425, GBM-1426, AA-1430, AA-1431, AA-1433, GBM-1445, and AA-1449 were derived from FIG-ROS InkΔ2/3 tumor cell lines. Identical amounts of proteins from each cell line were separated by SDS-PAGE and blotted against the indicated antibodies.

the SHP-2 interaction shown above, we transferred the two-dimensional gels and did a Western blot analysis using an anti-SHP-2 antibody (Fig. 4*B, right*), confirming the identity of the unknown phospho-62 kDa in our two-dimensional experiment as SHP-2. Tyrosine phosphorylation of SHP-2 has been shown to be confined to two residues within the COOH-terminal tail of the protein (26). To determine if any of these residues are phosphorylated in FIG-ROS-expressing cells, we immunoblotted lysates from Rat1 clones expressing FIG-ROS with phosphospecific SHP-2 antibodies (Supplementary Fig. S6). In cells expressing wild-type FIG-ROS but not in parental Rat1 cells, SHP-2 is phosphorylated on tyrosine residues Y542 and Y580. Taken together, the above results show that SHP-2 interacts with FIG-ROS and is a bona fide substrate for this kinase, and that this interaction and phosphorylation event parallels FIG-ROS ability to transform cells.

SHP-2 is phosphorylated in FIG-ROS-derived primary astrocytoma cell lines. To determine whether the observed FIG-ROS-mediated phosphorylation of SHP-2 in Rat1 cells reflected a signaling event applicable to astrocytomas, we established primary cultured cells from a series of tumors from FIG-ROS;InkΔ2/3 mice. These cells are capable of reconstituting the histologic features observed in the original astrocytoma when orthotopically grafted into the brains of nonobese diabetic/severe combined immunodeficient mice (Supplementary Fig. S7*A* and *B*) and proliferate indefinitely under standard culture conditions (Supplementary Fig. S7*C*). Figure 4*D* shows by Western blot analysis with anti-pY542 and anti-pY580 SHP-2 antibodies that astrocytoma cell lines derived from FIG-ROS;InkΔ2/3 tumors exhibit SHP-2 phosphorylation on tyrosine residues Y542 and Y580. These phosphorylation events underline the relevance of these FIG-ROS astrocytoma cell lines to the study of signal transduction pathways emanating from oncogenic FIG-ROS kinase.

Akt/mTOR signaling pathway axis activation in FIG-ROS/InkΔ2/3 tumors and cell lines. It has been shown that growth factor receptors can relay signaling information to PI3K and Akt through an activation of SHP-2 (27–30). In addition, activation of the Akt signaling pathway is a common genetic lesion in malignant astrocytomas in humans (31–33). To determine if FIG-ROS;InkΔ2/3 astrocytoma tumors also contain activated forms of Akt, we did immunostaining on tumor sections using an antibody that recognizes a phosphorylated (Ser^{473}) activated version of Akt (Fig. 5*A*). The tumors were readily labeled by this antibody, revealing the presence of activated Akt within these cells. The downstream effectors of activated Akt are numerous (reviewed in ref. 34). Recent work by Dasgupta et al. (35) showed hyperactivation of the mTOR pathway in human and mouse brain tumors. Akt activates mTOR through at least two pathways. A direct phosphorylation of mTOR by activated Akt has been reported to modulate its activity (34, 36). In addition, Akt exerts its control on mTOR through the modulation of the tuberin/hamartin complex, which is a key negative regulator of mTOR and a potent controller of its activity (37). The best characterized

function of mTOR in mammalian cells is regulation of translation through modulation of phosphorylation of ribosomal S6 kinase and eukaryote initiation factor 4E binding protein 1, key regulators of protein translation. Enhanced mTOR function can be detected by an increased phosphorylation of ribosomal S6 kinase, which translates into an increase in the phosphorylation levels of the ribosomal S6 protein. We did immunostaining using an anti-phospho-S6(Ser$^{235/236}$) antibody on our tumors to ascertain the status of S6 protein phosphorylation. A strong staining within the tumors was observed (Fig. 5*B*). To validate these observations, we treated one of the FIG-ROS;InkΔ2/3 astrocytoma cell lines (AA-1433) with the mTOR inhibitor rapamycin and assessed the levels of phospho-S6 proteins by Western blot analysis. Figure 5*C* shows that rapamycin treatment of FIG-ROS;InkΔ2/3$^{-/-}$ cell line AA-1433 dramatically reduces the levels of phospho-S6. We further tested whether this reduction is through the axis PI3K/Akt/mTOR by treating cell line AA-1433 with an inhibitor of PI3K and assessing the levels of phospho-Akt by Western blot analysis. Inhibition of PI3K activity by treatment of AA-1433 cells with wortmanin abrogated the levels of both phospho-Akt and phospho-S6 protein (Fig. 5*C*). The effect of inhibition of mTOR signaling on proliferation of FIG-ROS tumor cells was tested by growth assay experiments under increasing amount of rapamycin. As shown in Fig. 6*A*, the growth of all four FIG-ROS derived tumor cell lines was inhibited in a dose-dependent manner by rapamycin. These results show that a PI3K/Akt/mTOR signaling pathway is activated by FIG-ROS both in tumors and in cells derived from them.

Inhibition of SHP-2 activity abrogrates FIG-ROS-induced PI3K/Akt/mTOR signaling. To ascertain the role that SHP-2 activation plays on the activation of PI3K in our astrocytoma model, we treated tumor derived cells with calpeptin, a known inhibitor of SHP-2 (38), and assessed the effect of SHP-2 inhibition on the activation of a PI3K/Akt/mTOR signaling by Western blot analysis. Treatment of FIG-ROS tumor cell line AA-1433 with calpeptin resulted in a marked reduction in the levels of phospho-Akt^{S473} and phospho-S6 proteins (Fig. 6*B*). These results strongly suggest that the activated levels of Akt and mTOR activity in the FIG-ROS tumor cell lines are modulated by the activity of SHP-2.

Discussion

Ectopic expression of the orphan RTK ROS has been reported in many tumors of the CNS and recently in lung and stomach cancers (39, 40). These observations strongly suggest that ROS plays a role in tumorigenesis. This notion, however, remains, until now, unsubstantiated. We presented results herein that support, for the first time, the role of this RTK in cancer in an *in vivo* model of glioblastoma. We showed that expression of a constitutively active, ligand-independent ROS kinase in conjunction with the loss of the tumor suppressor *p16Ink4a;p19Arf* locus is sufficient to form malignant astrocytomas in a mouse model of brain cancer.

Expression of specific oncogenes in normal cells results either in apoptosis or in senescence, the latter being triggered by activating a series of molecular pathways involving key cancer proteins such as p53 or p19Arf (reviewed in ref. 41). Expression of FIG-ROS alone may induce senescence in normal cells, a hypothesis consistent with the relatively low rate of tumor formation in pCAGGS-LSL-FIG-ROS mice alone. Deleting the integral senescence protein p19Arf in InkΔ2/3 null animals may short-circuit such oncogene-induced senescence and allow for FIG-ROS-mediated transformation to take place in these cells. This duality seems to be specific to particular oncogenes and certain tissues. For example, preliminary results from our laboratory show that AdCre-mediated *in situ* activation of oncogenic k-Ras^{G12D} on a InkΔ2/3 null background does not lead to tumor formation (data not shown) whereas expression of FIG-ROS in the same context does. In addition, it has been shown that deletion of p19Arf in a model of activated Ras/Akt–induced astrocytoma revealed the importance of this senescence marker protein in tumor formation whereas it failed to do so in a model of SV40 large T antigen–induced choroid plexus carcinoma (42, 43). These results undeniably show the complexity of oncogenic mechanisms selected by tumor cells to overcome the natural cellular anticancer response that is senescence. The manipulability of our model system offers an unparalleled platform to do rigorous assessments of the genetic components crucial for this phenomenon.

The most impenetrable aspect to therapeutic intervention of malignant astrocytomas is their migrating nature, making full surgical resection physically impossible. Invading glioma cells seem to follow distinct anatomic structures within the central nervous system often egressing along white matter tracts, the basement membranes of blood vessels, or beneath the subdural sheets. We consistently observed migration of FIG-ROS;InkΔ2/3 astocytoma cells within the subdural and along vascular spaces. The extracellular milieu of anatomic structures, such as blood vessel

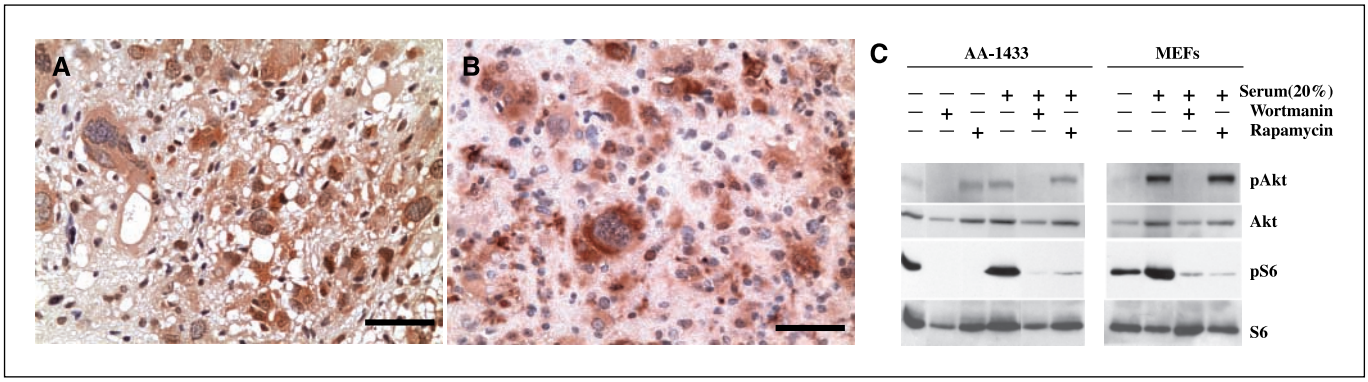

Figure 5. A PI3K/Akt/mTOR signaling pathway axis is activated in FIG-ROS-derived high-grade astrocytoma tumors. FIG-ROS;InkΔ2/3 null anaplastic astrocytoma and glioblastoma tumors stained positive for phospho-Akt^{Ser473} (*A*) and phospho-S6 protein (*B*). *C,* Western blot analysis of cell lysates from a FIG-ROS;InkΔ2/3 null anaplastic astrocytoma cell line 1433 and wild-type mouse embryonic fibroblast cells (*MEFs*) showing that the levels of phospho-Akt^{Ser473} and phospho-S6 are attenuated by the PI3K inhibitor wortmanin and the mTOR inhibitor rapamycin. Bar, 50 μm.

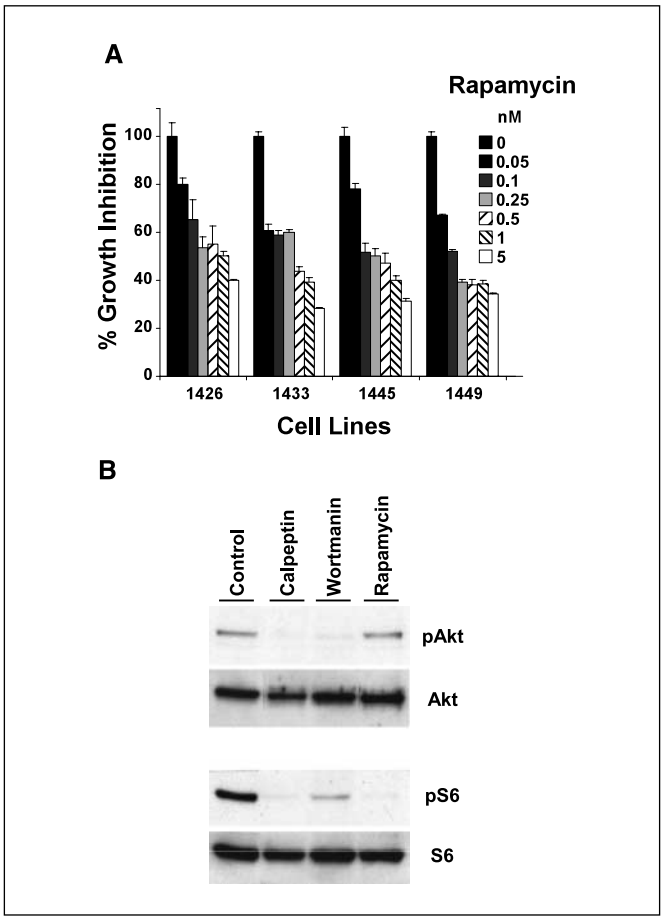

Figure 6. FIG-ROS malignant astrocytoma cell lines are sensitive to the mTOR inhibitor rapamycin and SHP-2 inhibitor calpeptin. *A,* dose-dependent inhibition of FIG-ROS;InkΔ2/3 null cell line growth by rapamycin. Growth assays were done in triplicate; *bars,* SD. *B,* FIG-ROS;InkΔ2/3 null cell line AA-1433 was treated with vehicle (*control*), 1 mmol/L of calpeptin, 1 μmol/L wortmanin, or 50 nmol/L rapamycin, and total cell lysates were blotted against phospho-Akt^{Ser473} and phospho-S6 ribosomal protein. Membranes were stripped and reprobed for total Akt and S6 proteins.

basement membranes or between myelinated axons, is profoundly different. This suggests a pleotropic fashion by which glioma cells are able to use a variety of matrix ligands, possibly activating distinct mechanisms for invasion. In this regard, we showed that FIG-ROS astrocytoma cells exhibit a preference for the subdural and perivascular spaces over white matter tracts as conduits for migration. This likely reflects the ability of FIG-ROS to activate specific mechanisms of invasion inherent to its signaling events in migrating cells, thus providing an excellent system to study modalities of astrocytoma cell invasion with respect to ROS activation in an *in vivo* model of glioblastoma multiforme.

The single most determining factor for prognosis for human glioblastoma multiforme is the age of the patient at diagnosis (1). This suggests an increased permissiveness of tumor growth in older patients. This observation has recently been reproduced experimentally using an orthotopic xenograft model of human glioblastoma multiforme (44), leading the authors to postulate that older animals have a reduced capacity for tumor growth suppression. We observed a significant difference in our cohort of FIG-ROS;InkΔ2/3 null animals: older mice succumbed to tumors more rapidly than younger animals (Supplementary Fig. S2*B*). This observation is likely not attributable to age differences in the rates of Cre-mediated excision *in vivo* because we have consistently observed similar rates of excision in reporter strain animals of various age (data not shown). The precise spatio-temporal induction of tumor growth in our model is well suited to mechanistically define parenchymal tissue reactivity towards tumor cell growth.

Signaling. Phosphorylation of SHP-2 on its COOH-terminal tail tyrosine residues Y542 and Y580 as well as its SH2 domain–mediated binding to tyrosine-phosphorylated proteins have been shown to enhance its phosphatase activity (reviewed in ref. 26). Our data show that both Y805 and Y865 of FIG-ROS are binding sites for the NH_2-terminal SH2 domain of SHP-2. Not surprisingly, both sites are surrounded by similar key position amino acid residues necessary for SHP-2 NH_2-terminal SH2 domain recognition, hydrophobic amino acid residues at positions pY +1 and +3 and valine/isoleucine/leucine at position −2 pY. Given that the COOH-terminal SH2 domain of SHP-2 binds an identical phosphotyrosine motif as the NH_2-terminal SH2 domain and that both Y805 and Y865 have the same +1, +3, and −2 residues, it is conceivable that both SH2 domains of SHP-2 bind simultaneously to Y805 and Y865 phosphorylated FIG-ROS. Concurrent occupation of the tandem SH2 repeats of SHP-2 by a dually phosphorylated ligand has been suggested (45–47) and confirmed (48) to confer enhanced biological activity in other RTK signaling systems. In addition, phosphorylation on SHP-2 COOH-terminal tail tyrosine residues (Y542 and Y580) has been proposed to act as an adapter function to recruit additional proteins, such as growth factor receptor binding protein 2 and SH2 domain–containing inositol phosphatase, through their SH2 domains and/or to directly regulate the phosphatase activity (26). Together, our results show that constitutively activated FIG-ROS interacts with and phosphorylates SHP-2 in a manner that promotes a sustained activation of the catalytic activity and function of SHP-2.

Downstream effectors of SHP-2 activation. SHP-2 has been shown to positively regulate the ability of several receptor kinases to activate the Ras/Raf/mitogen-activated protein kinase (MAPK) signaling cascade (reviewed in ref. 49). In most cases, the catalytic activity of SHP-2 is required to propagate receptor-mediated signaling to MAPK. We did not detect any elevated levels of phospho-Erk1/2 in cell lysates from FIG-ROS;InkΔ2/3 null tumor-derived cell lines (data not shown), indicating that FIG-ROS activation of SHP-2 does not result in Erk-mediated signaling events in these cells.

Growth factor receptor–mediated activation of SHP-2 has recently been shown to promote growth of glioblastoma cells in culture (28) and the activation of a PI3K/Akt signaling axis (27–30). Our immunohistochemical data and pharmacologic manipulation of SHP-2 activity provide evidence that activation of SHP-2 results in the activation of PI3K and Akt proteins. Recent work by Dasgupta et al. (35) showed that hyperactivation of the mTOR protein signaling pathway is a major event in human and mouse brain tumors. We show that activated Akt results in an increase in the ability of mTOR to enhance translational capacity. The increased levels of phospho-S6 proteins within FIG-ROS;InkΔ2/3 null tumors and cell cultures and the dependency of this increase on mTOR and PI3K function, as shown by rapamycin and wortmanin sensitivity, reveal a link between activated FIG-ROS and the PI3K/Akt/mTOR pathway, which is mediated by SHP-2 activity. Moreover, inhibition of mTOR protein by rapamycin resulted in a dose-dependent inhibition of FIG-ROS;InkΔ2/3 null

cell cultures growth. This axis has particular clinical relevance because inhibitors of mTOR protein are currently undergoing oncology clinical trials. Our data show that tumors expressing activated ROS or SHP-2 mutant alleles should be considered for treatment with these targeted therapeutics.

Conclusion. Understanding cellular transformation by FIG-ROS and the signaling systems necessary for this event may have broad implications for therapeutic interventions of malignant astrocytomas because ectopic expression of ROS in human brain tumors is frequently observed. The results presented here clearly show that FIG-ROS and SHP-2 activation contributes to oncogenesis in solid tumors of this type. Given the recent discoveries that constitutively activated SHP-2 promotes hematologic malignancy in animals and the presence of mutated *Shp-2* alleles in solid tumors of various cancer types, our identification of a novel SHP-2 activator is particularly important vis-a-vis understanding tumorigenesis. The results obtained from our model show for the first time that constitutive activation of SHP-2 parallels solid tumor formation and suggest an alternative path to therapeutic intervention. In addition, our demonstration that activated ROS receptor is capable of initiating tumorigenesis *in vivo* provides a novel therapeutic target for the management of glioblastomas.

Acknowledgments

Received 4/3/2006; revised 5/18/2006; accepted 6/2/2006.

Grant support: National Cancer Institute of Canada and the Canadian Institutes of Health Research (A. Charest), the Virginia and DK Ludwig Fund for Cancer Research (D. Housman and T. Jacks), and NIH grants P01 CA-042063 (D. Housman) and RO1 GM-060594 (M.B. Yaffe).

The costs of publication of this article were defrayed in part by the payment of page charges. This article must therefore be hereby marked *advertisement* in accordance with 18 U.S.C. Section 1734 solely to indicate this fact.

We thank Drs. Jill Crittenden, Ruth Bodner, and Marius Werning for critical review of the manuscript.

References

1. Ohgaki H, Kleihues P. Epidemiology and etiology of gliomas. Acta Neuropathol (Berl) 2005;109:93–108.
2. Liu ZZ, Wada J, Kumar A, Carone FA, Takahashi M, Kanwar YS. Comparative role of phosphotyrosine kinase domains of c-ros and c-ret proto-oncogenes in metanephric development with respect to growth factors and matrix morphogens. Dev Biol 1996;178: 133–48.
3. Sonnenberg E, Godecke A, Walter B, Bladt F, Birchmeier C. Transient and locally restricted expression of the ros1 proto-oncogene during mouse development. EMBO J 1991;10:3693–702.
4. Tessarollo L, Nagarajan L, Parada LF. c-ros: the vertebrate homologue of the sevenless tyrosine kinase receptor is tightly regulated during organogenesis in mouse embryonic development. Development 1992;115: 11–20.
5. Birchmeier C, Sharma S, Wigler M. Expression and rearrangement of the ROS1 gene in human glioblastoma cells. Proc Natl Acad Sci U S A 1987;84:9270–4.
6. Sharma S, Birchmeier C, Nikawa J, O'Neill K, Rodgers L, Wigler M. Characterization of the ros1-gene products expressed in human glioblastoma cell lines. Oncogene Res 1989;5:91–100.
7. Wu JK, Chikaraishi DM. Differential expression of ros oncogene in primary human astrocytomas and astrocytoma cell lines. Cancer Res 1990;50:3032–5.
8. Mapstone T, McMichael M, Goldthwait D. Expression of platelet-derived growth factors, transforming growth factors, and the ros gene in a variety of primary human brain tumors. Neurosurgery 1991;28:216–22.
9. Watkins D, Dion F, Poisson M, Delattre JY, Rouleau GA. Analysis of oncogene expression in primary human gliomas: evidence for increased expression of the ros oncogene. Cancer Genet Cytogenet 1994;72: 130–6.
10. Zhao JF, Sharma S. Expression of the ROS1 oncogene for tyrosine receptor kinase in adult human meningiomas. Cancer Genet Cytogenet 1995;83:148–54.
11. Charest A, Kheifets V, Park J, et al. Oncogenic targeting of an activated tyrosine kinase to the Golgi apparatus in a glioblastoma. Proc Natl Acad Sci U S A 2003;100:916–21.
12. Charest A, Lane K, McMahon K, et al. Fusion of FIG to the receptor tyrosine kinase ROS in a glioblastoma with an interstitial del(6)(q21q21). Genes Chromosomes Cancer 2003;37:58–71.
13. Choong K, Freedman MH, Chitayat D, Kelly EN, Taylor G, Zipursky A. Juvenile myelomonocytic leukemia and Noonan syndrome. J Pediatr Hematol Oncol 1999; 21:523–7.
14. Loh ML, Vattikuti S, Schubbert S, et al. Mutations in PTPN11 implicate the SHP-2 phosphatase in leukemogenesis. Blood 2004;103:2325–31.
15. Tartaglia M, Niemeyer CM, Fragale A, et al. Somatic mutations in PTPN11 in juvenile myelomonocytic leukemia, myelodysplastic syndromes and acute myeloid leukemia. Nat Genet 2003;34:148–50.
16. Tartaglia M, Martinelli S, Cazzaniga G, et al. Genetic evidence for lineage-related and differentiation stage-related contribution of somatic PTPN11 mutations to leukemogenesis in childhood acute leukemia. Blood 2004;104:307–13.
17. Tartaglia M, Niemeyer CM, Shannon KM, Loh ML. SHP-2 and myeloid malignancies. Curr Opin Hematol 2004;11:44–50.
18. Bentires-Alj M, Paez JG, David FS, et al. Activating mutations of the Noonan syndrome-associated SHP2/PTPN11 gene in human solid tumors and adult acute myelogenous leukemia. Cancer Res 2004;64:8816–20.
19. Mohi MG, Williams IR, Dearolf CR, et al. Prognostic, therapeutic, and mechanistic implications of a mouse model of leukemia evoked by Shp2 (PTPN11) mutations. Cancer Cell 2005;7:179–91.
20. Miyazaki J, Takaki S, Araki K, et al. Expression vector system based on the chicken β-actin promoter directs efficient production of interleukin-5. Gene 1989;79:269–77.
21. Serrano M, Lee H, Chin L, Cordon-Cardo C, Beach D, DePinho RA. Role of the INK4a locus in tumor suppression and cell mortality. Cell 1996;85:27–37.
22. Charest A, Lane K, McMahon K, Housman DE. Association of a novel PDZ domain-containing peripheral Golgi protein with the Q-SNARE (Q-soluble N-ethylmaleimide-sensitive fusion protein (NSF) attachment protein receptor) protein syntaxin 6. J Biol Chem 2001;276:29456–65.
23. Ausubel F, Brent R, Kingston RE, et al. In: Ausubel F, Brent R, Kingston RE Moore DD, Seidman JG, Smith JA, Struhl K, editors. Current protocols in molecular biology. New York: John Wiley & Sons, Inc.; 2001.
24. Kleihues P, Sobin LH. World Health Organization classification of tumors. Cancer 2000;88:2887.
25. Pawson T. Specificity in signal transduction: from phosphotyrosine-SH2 domain interactions to complex cellular systems. Cell 2004;116:191–203.
26. Poole AW, Jones ML. A SHPing tale: perspectives on the regulation of SHP-1 and SHP-2 tyrosine phosphatases by the C-terminal tail. Cell Signal 2005; 17:1323–32.
27. Zhang SQ, Tsiaras WG, Araki T, et al. Receptor-specific regulation of phosphatidylinositol 3′-kinase activation by the protein tyrosine phosphatase Shp2. Mol Cell Biol 2002;22:4062–72.
28. Wu CJ, O'Rourke DM, Feng GS, Johnson GR, Wang Q, Greene MI. The tyrosine phosphatase SHP-2 is required for mediating phosphatidylinositol 3-kinase/Akt activation by growth factors. Oncogene 2001;20: 6018–25.
29. Hakak Y, Hsu YS, Martin GS. Shp-2 mediates v-Src-induced morphological changes and activation of the anti-apoptotic protein kinase Akt. Oncogene 2000;19: 3164–71.
30. Ivins Zito C, Kontaridis MI, Fornaro M, Feng GS, Bennett AM. SHP-2 regulates the phosphatidylinositide 3′-kinase/Akt pathway and suppresses caspase 3-mediated apoptosis. J Cell Physiol 2004; 199:227–36.
31. Hu X, Pandolfi PP, Li Y, Koutcher JA, Rosenblum M, Holland EC. mTOR promotes survival and astrocytic characteristics induced by Pten/AKT signaling in glioblastoma. Neoplasia 2005;7:356–68.
32. Haas-Kogan D, Shalev N, Wong M, Mills G, Yount G, Stokoe D. Protein kinase B (PKB/Akt) activity is elevated in glioblastoma cells due to mutation of the tumor suppressor PTEN/MMAC. Curr Biol 1998;8: 1195–8.
33. Holland EC, Celestino J, Dai C, Schaefer L, Sawaya RE, Fuller GN. Combined activation of Ras and Akt in neural progenitors induces glioblastoma formation in mice. Nat Genet 2000;25:55–7.
34. Bellacosa A, Kumar CC, Cristofano AD, Testa JR. Activation of AKT kinases in cancer: implications for therapeutic targeting. Adv Cancer Res 2005;94: 29–86.
35. Dasgupta B, Yi Y, Chen DY, Weber JD, Gutmann DH. Proteomic analysis reveals hyperactivation of the mammalian target of rapamycin pathway in neurofibromatosis 1-associated human and mouse brain tumors. Cancer Res 2005;65:2755–60.
36. Sekulic A, Hudson CC, Homme JL, et al. A direct linkage between the phosphoinositide 3-kinase-AKT signaling pathway and the mammalian target of rapamycin in mitogen-stimulated and transformed cells. Cancer Res 2000;60:3504–13.
37. Inoki K, Corradetti MN, Guan KL. Dysregulation of the TSC-mTOR pathway in human disease. Nat Genet 2005;37:19–24.
38. Schoenwaelder SM, Petch LA, Williamson D, Shen R, Feng GS, Burridge K. The protein tyrosine phosphatase Shp-2 regulates RhoA activity. Curr Biol 2000;10:1523–6.
39. Yamashita S, Nomoto T, Abe M, Tatematsu M, Sugimura T, Ushijima T. Persistence of gene expression changes in stomach mucosae induced by short-term *N*-methyl-*N*′-nitro-*N*-nitrosoguanidine treatment and their presence in stomach cancers. Mutat Res 2004;549:185–93.
40. Sweet-Cordero A, Mukherjee S, Subramanian A, et al. An oncogenic KRAS2 expression signature identified by cross-species gene-expression analysis. Nat Genet 2005; 37:48–55.
41. Itahana K, Campisi J, Dimri GP. Mechanisms of cellular senescence in human and mouse cells. Biogerontology 2004;5:1–10.

42. Tolbert D, Lu X, Yin C, Tantama M, Van Dyke T. p19(ARF) is dispensable for oncogenic stress-induced p53-mediated apoptosis and tumor suppression in vivo. Mol Cell Biol 2002;22:370–7.
43. Uhrbom L, Kastemar M, Johansson FK, Westermark B, Holland EC. Cell type-specific tumor suppression by Ink4a and Arf in Kras-induced mouse gliomagenesis. Cancer Res 2005;65:2065–9.
44. Glass R, Synowitz M, Kronenberg G, et al. Glioblastoma-induced attraction of endogenous neural precursor cells is associated with improved survival. J Neurosci 2005;25:2637–46.
45. Eck MJ, Pluskey S, Trub T, Harrison SC, Shoelson SE. Spatial constraints on the recognition of phosphoproteins by the tandem SH2 domains of the phosphatase SH-PTP2. Nature 1996;379:277–80.
46. Hof P, Pluskey S, Dhe-Paganon S, Eck MJ, Shoelson SE. Crystal structure of the tyrosine phosphatase SHP-2. Cell 1998;92:441–50.
47. Ottinger EA, Botfield MC, Shoelson SE. Tandem SH2 domains confer high specificity in tyrosine kinase signaling. J Biol Chem 1998;273:729–35.
48. Cunnick JM, Mei L, Doupnik CA, Wu J. Phosphotyrosines 627 and 659 of Gab1 constitute a bisphosphoryl tyrosine-based activation motif (BTAM) conferring binding and activation of SHP2. J Biol Chem 2001;276:24380–7.
49. Neel BG, Gu H, Pao L. The "Shp"ing news: SH2 domain-containing tyrosine phosphatases in cell signaling. Trends Biochem Sci 2003;28:284–93.